Polymer 84 (2016) 355–364

Contents lists available at ScienceDirect

Polymer

journal homepage: www.elsevier.com/locate/polymer

Effects of main chain and acceptor content on phase behaviors of hydrogen-bonded main-chain/side-chain combined liquid crystalline polymers

Shuai-Qi Yang [a, b, 1], Wei Qu [a, 1, 2], Hong-Bing Pan [a], Yu-Dong Zhang [a], Shi-Jun Zheng [b, **], Xing-He Fan [a], Zhihao Shen [a, *]

[a] Beijing National Laboratory for Molecular Sciences, The Key Laborarotary of Polymer Chemistry and Physics of Ministry of Education, Center for Soft Matter Science and Engineering, College of Chemistry and Molecular Engineering, Peking University, Bejing 100871, China
[b] College of Materials Science and Engineering, Zhengzhou University, Zhengzhou 450000, China

ARTICLE INFO

Article history:
Received 27 August 2015
Received in revised form
1 January 2016
Accepted 6 January 2016
Available online 8 January 2016

Keywords:
Main-chain/side-chain combined liquid crystalline polymer
Hydrogen-bonding
Hierarchical structure

ABSTRACT

Main-chain/side-chain combined liquid crystalline polymers (MCSCLCPs) are usually difficult to synthesize and their degrees of polymerization are relatively low, which bring difficulties in studying their structure–property relationships. In order to solve this problem, we prepared a new series of MCSCLCPs containing mesogen-jacketed liquid crystalline polymer (MJLCP) main chains via hydrogen-bonding (H–B). A pyridine derivative with a triphenylene (Tp) unit is the H–B acceptor. In addition to the temperature dependence, the phase behavior of the resulting complex is strongly influenced by the content of the H–B acceptor and the rigidity of the side-chain core of the MJLCP. The resulting complexes exhibit different phase structures: (1) a columnar nematic phase or a smectic A (SmA) phase formed by the supramolecular MJLCP chain as a whole; (2) hierarchical nanostructures including a hexagonal columnar phase or a SmA phase of the whole polymer chain plus a discotic nematic phase associated with the Tp moieties.

1. Introduction

Liquid crystal (LC), a typical soft matter with mesophase structures between the three-dimensionally ordered crystal and isotropic liquid state, can exhibit phase structures with one-dimensional (1D) or two-dimensional (2D) order on the length scale of about 1–10 nm. Liquid crystalline polymers (LCPs) have received much attention because of their potential applications in fields such as electro-optic materials, catalysis, nano-templates, etc. [1–6]. In the past decades, scientists have paid attention to the strategies in the design and synthesis of LCPs by selecting different mesogenic groups, varying the location of the mesogen, changing the length of the flexible spacer, and so on, in order to obtain more controllable and complex structures [7–10]. Main-chain/side-chain combined LCP (MCSCLCP), a hybrid structure which combines the chemical features of both main-chain liquid crystalline polymer (MCLCP) and side-chain liquid crystalline polymer (SCLCP), may have more complex phase behaviors compared to conventional MCLCPs and SCLCPs [11]. Since the first example reported by Ringsdorf et al. [12], many MCSCLCPs have been synthesized and investigated [13–16]. Generally, in MCSCLCPs, the main chain is a rigid rod or rod-like chain composed of mesogenic groups and flexible spacers, while the side chain usually contains a mesogenic group linked to the main-chain repeating unit through a flexible spacer. The typical method to obtain this kind of MCSCLCP is condensation polymerization, and thus the molecular weight (MW) and the polydispersity index (PDI) of the polymer are not easily controllable.

Mesogen-jacketed liquid crystalline polymers (MJLCPs) are, chemically speaking, SCLCPs with a very short spacer or a single carbon–carbon bond between the backbone and the laterally attached bulky side group [17,18]. The "jacketing" effect or the steric effect makes the backbone of the MJLCP more or less extended, and

---

* Corresponding author.
** Corresponding author.
E-mail addresses: zsj316@zzu.edu.cn (S.-J. Zheng), zshen@pku.edu.cn (Z. Shen).
[1] These two authors contributed equally.
[2] Current address: Research Institute of Wood Industry, Chinese Academy of Forestry, CRIWI, No. 2, Dongxiaofu, Xiangshan Road, Haidian District, Beijing 100091, China.

http://dx.doi.org/10.1016/j.polymer.2016.01.018
0032-3861/© 2016 Elsevier Ltd. All rights reserved.

the polymer chain as a whole acts like a supramolecular rod. Therefore, MJLCPs are more like MCLCPs rather than SCLCPs from a physical point of view. Xie et al. investigated an MCSCLCP based on an MJLCP main chain, poly(2,5-bis{[6-(4-butoxy-40-oxy-biphenyl) hexyl]oxycarbonyl}styrene) (PBBHCS), which was synthesized using free radical polymerization [19]. Biphenyl groups are incorporated into the side chain. At low temperatures PBBHCS exhibits a hierarchical supramolecular structure with double orderings on different length scales. The main chain constructs a rectangular scaffold on the nanometer length scale, and the biphenyl-containing side chains form a smectic E (SmE)-like structure on the subnanometer length scale [20]. Zhu et al. studied another MJLCP-based MCSCLCP PP*n*V, which incorporates triphenylene (Tp) units into the side chain [21,22]. PPnV also exhibits hierarchical supramolecular structures in which the main chain forms the columnar structure and the Tp units in the side chain form a discotic nematic (N_D) phase. However, the MW of the monomer of PPnV is high, and the fraction of the polymerizable styrene unit is relatively low in the monomer, both of which will lead to a smaller degree of polymerization (DP) in preparation by atom transfer radical polymerization (ATRP). It brings difficulties in studying the structure–property relationship of this and other similar MCSCLCPs.

Another useful and simple method to building LCPs is via hydrogen bonding. During the past few decades, main-chain, side-chain, and network LCPs have been designed and prepared by using hydrogen bonding [23–28]. Xu et al. synthesized a new series of MJLCPs, utilizing hydrogen bonding, and the resulting complexes form a smectic A (SmA) or columnar nematic (Col_n) phase [29]. Huang et al. prepared hydrogen-bonded MCSCLCPs with a pyridine group-containing MCLCP and two ligands having the carboxylic acid group (–COOH), and they investigated the influence of the side-chain mesogen on the phase behavior of the MCSCLCPs [15]. However, to the best of our knowledge, the influence of main-chain mesogen on the phase behavior of MCSCLCPs prepared via hydrogen bonding has never been investigated. Therefore, the design and preparation of new MCSCLCPs based on different MJLCP main chains using hydrogen bonding are appealing and promising.

In this work, we designed and prepared new hydrogen-bonded MCSCLCPs (see Chart 1) based on MJLCP main chains. The main chains, which are used as the hydrogen-bonding donors, are two mesogen-jacketed polyelectrolytes (MJPEs) containing two –COOH groups in the side chain, poly(vinyl terephthalic acid) (PVTA) and poly[2,5-bis(4-carboxylic phenyl)styrene] (PBCPS). And a pyridine derivative containing a Tp unit, 4-(6-(3,6,7,10,11-pentakis(hexyloxy)triphenylen-2-yloxy)hexyloxy)pyridine ($PHTC_6$, where 6 is the number of the methylene units between pyridine and Tp) is the hydrogen-bonding acceptor. One of our objectives is to explore the possibility of preparing MCSCLCPs based on MJLCP main chains via hydrogen bonding. The other objective is to study the influences of the main chain and the content of the pyridine derivative on the phase behaviors of these MCSCLCPs.

Self-assembled phase structures of the MJPE-ligand complexes in bulk were investigated using various techniques. The complexes with different compositions are denoted as $PVTA(PHTC_6)_x$ and $PBCPS(PHTC_6)_x$ (where the value of x indicates the molar ratio of $PHTC_6$ to the –COOH group in the MJPE repeating unit). We mainly focused on complexes with x ranging from 0.5 to 1, where macrophase separation did not occur.

2. Materials and methods

2.1. Materials

Dimethyl formamide (DMF) was refluxed over potassium hydroxide and distilled out before use. Tetrahydrofuran (THF) was refluxed over sodium under argon and distilled before use. Chlorobenzene was washed by H_2SO_4 and then distilled under a reduced pressure. All other reagents were used as received from commercial sources.

2.2. Measurements

All the measurements, such as ^1H NMR spectrometry, mass spectrometry (MS), gel permeation chromatography (GPC), thermogravimetric analysis (TGA), differential scanning calorimetry (DSC), FTIR spectroscopy, polarized light microscopy (PLM), small-angle X-ray scattering (SAXS), and 2D wide-angle X-ray diffraction (WAXD) experiments, were performed according to the procedures previously described [30,31].

2.3. Synthesis of the MJPEs

The chemical structures and synthetic procedures of the monomers and polymers are illustrated in Scheme 1. The experimental details are described as follows.

2.3.1. Synthesis of di-tert-butyl 2-vinylterephthalate (TBVT)

2-Vinylbenzene-1,4-dioic acid was synthesized according to the procedure reported previously [32]. 2-Vinylbenzene-1,4-dioic acid (1.92 g, 10.0 mmol), 2-methylpropan-2-ol (2.22 g, 30.0 mmol), *N*,*N*′-dicyclohexylcarbodiimide (DCC, 10.6 g, 50.0 mmol), *N*,*N*-dimethylpyridin-4-amine (DMAP, 0.120 g, 1.00 mmol), and 50 mL of dry dichloromethane were added into a 100 mL round-bottomed flask, and then the mixture was stirred at ambient temperature for 24 h. The insoluble material was removed by filtration, and the solvent was evaporated under a reduced pressure. The product was purified by passing through a silica gel column with dichloromethane and petroleum ether (v:v, 1:3) as the eluent. The obtained monomer was a light yellow liquid. ^1H NMR (400 MHz, $CDCl_3$, δ, ppm): 1.67 (s, 18H), 5.37–5.41 (d, 1H), 5.70–5.76 (d, 1H), 7.33–7.43 (p, 1H), 7.80–7.82 (d, 1H), 7.87–7.90 (d, 1H), 8.16 (s, 1H). MS (EI, m/z): 304.2 ($M^{\cdot+}$).

2.3.2. Synthesis of methyl 4-(4,4,5,5-tetramethyl-1,3,2-dioxaborolan-2-yl)benzoate

2,5-Dibromostyrene was synthesized according to the previously reported method [33]. 4-(Methoxycarbonyl)phenylboronic

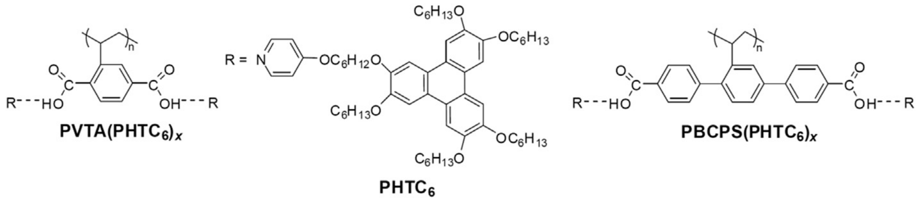

Chart 1. Chemical structures of the supramolecular MCSCLCPs.

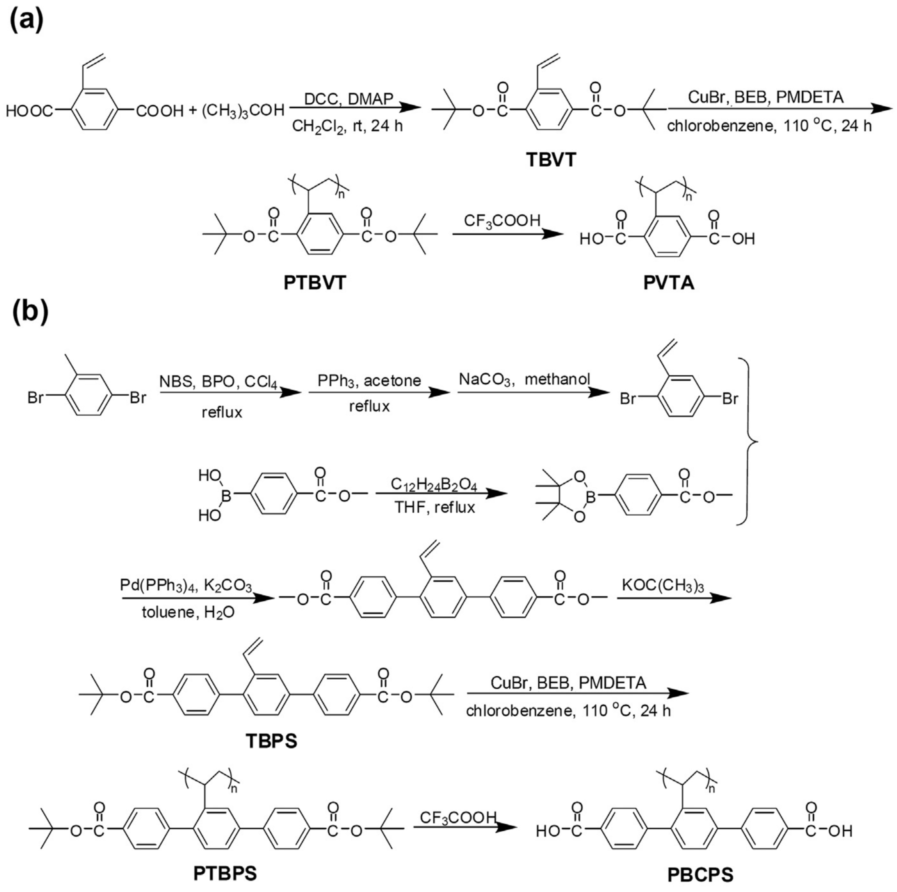

Scheme 1. Synthetic route of PVTA (a) and PBCPS (b).

acid (20.5 g, 114 mmol), 2,3-dimethyl-2,3-butanediol (14.0 g, 118 mmol), and 500 mL of dry THF were added into a 1000 mL round-bottomed flask, and then the mixture was refluxed at 70 °C for 2 h. The solvent was evaporated under a reduced pressure, and the residue was purified by passing through an Al_2O_3 column with THF as the eluent. ^{1}H NMR (400 MHz, $CDCl_3$, δ, ppm): 3.89 (s, 3H), 5.34 (d, 2H), 5.44 (d, 2H), 7.24–7.446 (d, 1H), 7.57 (q, 1H), 7.66 (d, 1H).

2.3.3. Synthesis of 2,5-bis(4-methoxycarbonyl phenyl)styrene

2,5-Dibromostyrene (2.10 g, 4.23 mmol), 4-methyl-(4,4,5,5-tetramethyl-1,3,2-dioxaborolan-2-yl)benzoate (2.44 g, 9.30 mmol), potassium carbonate (5.84 g, 42.3 mmol), hydroquinone (0.130 g, 1.18 mmol), and $Pd(PPh_3)_4$ (0.150 g, 0.130 mmol) were added into a 100 mL three-necked flask. Then toluene (30.0 mL) and water (10.0 mL) were injected under a continuous stream of argon. The mixture was stirred at 110 °C for 48 h. The separated organic layer was dried using anhydrous $MgSO_4$. After the solvent was evaporated under a reduced pressure, the product was purified by passing through a silica gel column with ethyl acetate and petroleum ether (v:v, 1:10) as the eluent. ^{1}H NMR (400 MHz, $CDCl_3$, δ, ppm): 3.78–3.80 (s, 6H), 5.32–5.35 (d, 1H), 5.80–5.85 (d, 1H), 6.62–6.70 (q, 1H), 7.40–7.44 (d, 1H), 7.56–7.60 (d, 2H), 7.60–7.64 (q, 1H), 7.82–7.84 (d, 2H), 7.86–7.88 (d, 1H), 7.96–8.00 (d, 2H), 8.00–8.04 (d, 2H).

2.3.4. Synthesis of 2,5-bis(4-tert-btuoxylcarbonyl phenyl)styrene (TBPS)

2,5-Bis(4-methoxycarbonyl phenyl)styrene (3.70 g, 9.94 mmol) was dissolved in 150 mL of anhydrous ether, then potassium *tert*-butoxide (11.2 g, 99.8 mmol) was added slowly. The mixture was stirred at ambient temperature for another 2 h, washed with 300 mL of water, and dried using anhydrous $MgSO_4$. After filtration, the solvent was evaporated, and the residue was purified by passing through a silica gel column with CH_2Cl_2 and petroleum ether (v:v, 1:10). ^{1}H NMR (400 MHz, $CDCl_3$, δ, ppm): 0.5–1.6 (d, 18H), 5.32–5.35 (d, 1H), 5.80–5.85 (d, 1H), 6.62–6.70 (q, 1H), 7.40–7.44 (d, 1H), 7.56–7.60 (d, 2H), 7.60–7.64 (q, 1H), 7.82–7.84 (d, 2H), 7.86–7.88 (d, 1H), 7.96–8.00 (d, 2H), 8.00–8.04 (d, 2H). Anal. Calcd. for $C_{30}H_{32}O_4$ (%): C, 78.92; H, 7.06. Found: C, 78.98; H, 7.07. MS (EI, m/z): 456.2 ($M^{\cdot+}$).

2.3.5. Polymerization

The polymers were obtained by ATRP. Taking poly(di-*tert*-butyl 2-vinylterephthalate) (PTBVT) as an example, the detailed procedure was carried out as follows. The monomer TBVT (1.00 g, 3.28 mmol), *N*,*N*,*N*′,*N*″,*N*″-pentamethyldiethylenetriamine (PMDETA, 5.68 mg, 32.8 μmol), (1-bromoethyl)benzene (BEB, 6.07 mg, 32.8 μmol), CuBr (4.72 mg, 32.8 μmol), dry chlorobenzene (1.5 g), and a magnetic stir bar were added into a polymerization tube. After three freeze–pump–thaw cycles, the tube was sealed under vacuum and subsequently immerged into an oil bath thermostated at 110 °C for 24 h. The polymerization was stopped when the tube was quenched in liquid nitrogen and taken out to ambient conditions. The solution was diluted with THF (5 mL) and then passed through a neutral alumina column in order to remove copper salt. At last, the polymer was precipitated out from methanol and dried in vacuum overnight.

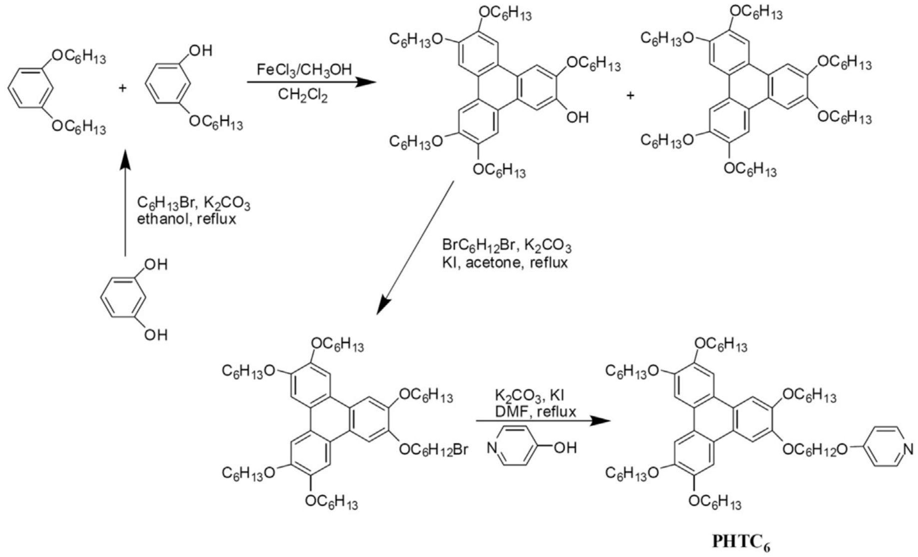

Scheme 2. Synthetic route of PHTC$_6$.

2.3.6. Synthesis of MJPEs

After 300 mg of the precursor polymer samples was dissolved in 10 mL of chloroform, 5 mL of trifluoroacetic acid was slowly added at ambient temperature. The solution was further stirred for 24 h, followed by the removal of the solvent under a reduced pressure. The residue was washed with ethyl ether for three times to obtain the pure product.

2.4. Synthesis of the Tp-containing pyridine derivative

The synthetic route of the pyridine derivative is depicted in Scheme 2. 2-Hydroxyl-3,6,7,10,11-pentakis(hexyloxy)triphenylene (PHT) was synthesized according to the reported procedure [34].

2.4.1. Synthesis of PHTC$_6$

PHT (4.50 g, 6.04 mmol), 1,6-dibromohexane (4.42 g, 18.1 mmol), potassium carbonate (1.24 g, 8.98 mmol), potassium iodide (0.100 g, 0.604 mmol), and acetonitrile (100 mL) were charged in a 250 mL three-necked flask. The mixture was refluxed for 24 h and then cooled to ambient temperature. After the resulting mixture was filtered, the solvent in the filtrate was removed under a reduced pressure. The residue was purified by passing through a silica gel column with ethyl acetate and petroleum ether (v:v, 1:15) as the eluent. Then the resultant product (5.95 g, 6.00 mmol), pyridin-4-ol (0.685 g, 7.20 mmol), potassium carbonate (2.49 g, 18.0 mmol), potassium iodide (0.100 g, 0.604 mmol), and DMF (100 mL) were charged in a 250 mL three-necked flask. The mixture was refluxed for 24 h and then cooled to ambient temperature. After the resulting mixture was filtered, the solvent in the filtrate was removed under a reduced pressure. The residue was purified by passing through a silica gel column with dichloromethane and methanol (v:v, 30:1) as the eluent. ^{1}H NMR (400 MHz, CDCl$_3$, δ, ppm): 0.87–0.97 (t, 15H), 1.32–1.44 (m, 22H), 1.52–1.61 (m, 10H), 1.64–1.70 (m, 2H), 1.87–1.98 (m, 14H), 4.20–4.30 (m, 14H), 7.47–7.54 (t, 2H), 7.77–7.87 (m, 6H), 8.06–8.13 (s, 2H). Anal. Calcd. for $C_{59}H_{87}NO_7$ (%): C, 76.83; H, 9.51; N, 1.52. Found: C, 76.50; H, 9.99; N, 1.56. MS (EI, m/z): 921.7 ($M^{\cdot+}$).

2.5. Preparation of the complexes

The complexes with different molar ratios of PHTC$_6$ to the —COOH group in the repeating unit were prepared using the pyridine solution. The MJPE and PHTC$_6$ were separately dissolved in pyridine solutions until clear solutions were obtained, and then the solutions were mixed together, followed by mechanical stirring at

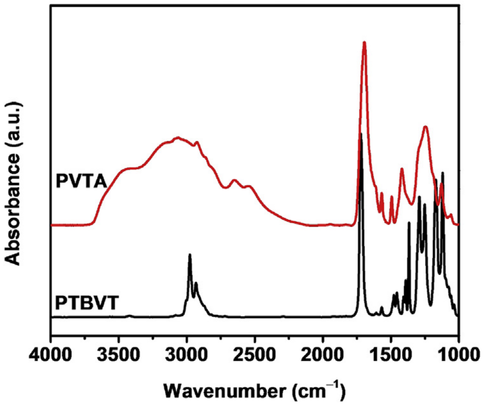

Fig. 1. FT-IR spectra of PTBVT and PVTA.

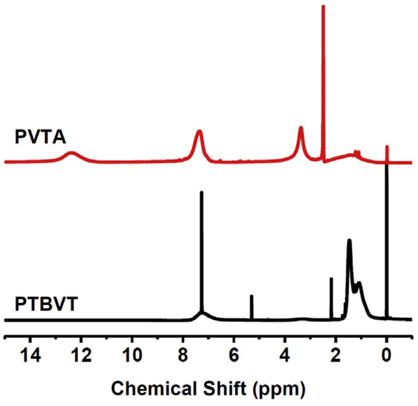

Fig. 2. ^{1}H NMR spectra of PTBVT and PVTA.

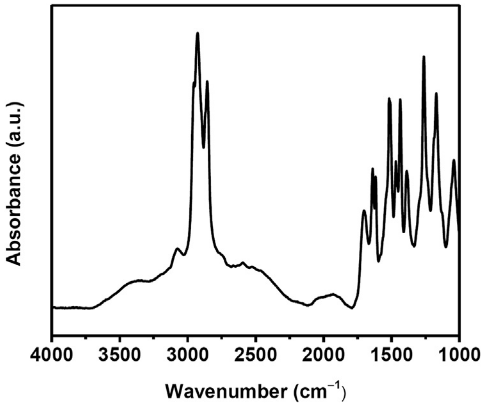

Fig. 3. FT-IR spectrum of PVTA($PHTC_6$)$_{0.5}$.

60 °C for about 24 h. The solution concentration was about 5 mg/mL to ensure the formation of a homogeneous solution. Afterwards, the solvent was allowed to slowly evaporate at 50 °C for about 3 days. Then the obtained complexes were further dried at 60 °C in vacuum for another 24 h to remove the residual solvent.

3. Results and discussion

3.1. Synthesis and characterization of the polymers and the hydrogen-bonded complexes

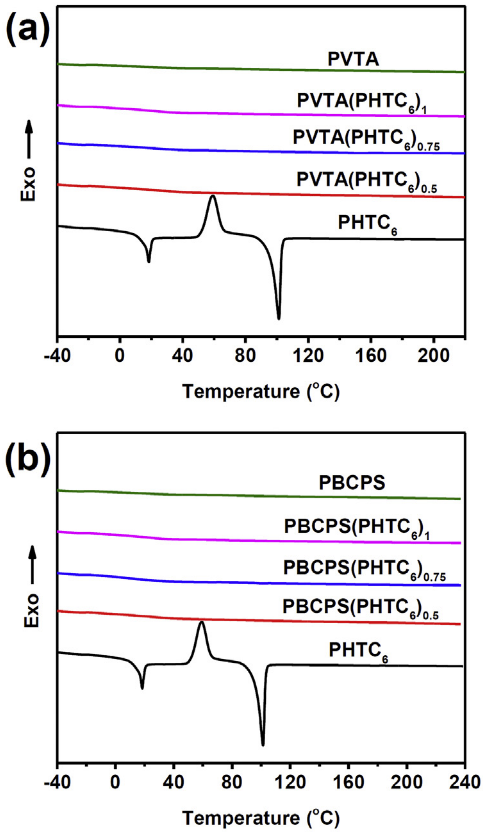

Fig. 4. DSC curves of PVTA($PHTC_6$)$_x$ (a) and PBCPS($PHTC_6$)$_x$ (b) along with those of PVTA, PBCPS, and $PHTC_6$ during the second heating at a rate of 10 °C/min under a N_2 atmosphere.

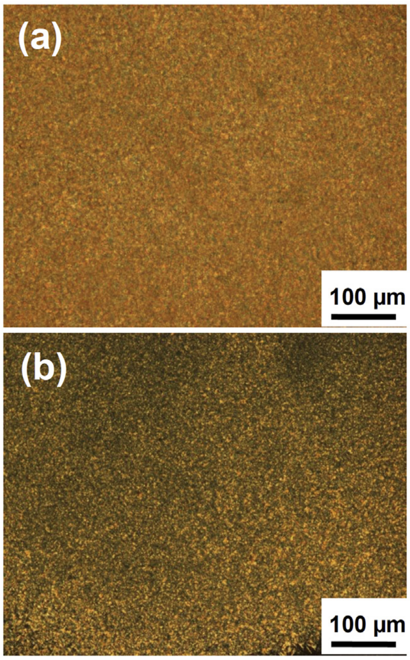

Fig. 5. Representative PLM micrographs of PVTA($PHTC_6$)$_1$ (a) and PBCPS($PHTC_6$)$_1$ (b) at 100 °C.

The structures of the monomers were confirmed by ^{1}H NMR and MS spectrometry. Polymers were obtained by ATRP, and the ratio of the monomer to the initiator was 100:1. Taking poly(di-*tert*-butyl 2-vinylterephthalate) (PTBVT) as an example, the GPC curve shows that the number-averaged MW (M_n) of PTBVT is 25.7 kDa and its PDI value is 1.11 (Fig. S1 in Supplementary Content). The complete removal of the neopentyl groups is confirmed by FT-IR and NMR results. For example, Fig. 1 shows the FT-IR spectra of PTBVT and PVTA. The vibration band at 1720 cm^{-1} for PTBVT shifts to 1695 cm^{-1} for PVTA, indicating that the neopentyl groups are removed and the $-COOC(CH_3)_3$ groups have changed to the $-COOH$ groups. The broad band between 2800 and 3700 cm^{-1} also proves the existence of the $-COOH$ groups [29]. In Fig. 2, the signals of the neopentyl groups in PTBVT at 1.46 ppm in the spectrum of PTBVT completely disappear in the spectrum of PVTA, demonstrating that the neopentyl groups are completely removed from PTBVT.

The formation of hydrogen bond between the carboxylic acid group of the MJPEs and the pyridine nitrogen of $PHTC_6$ was also investigated by FT-IR. For example, the FT-IR result of PVTA($PHTC_6$)$_{0.5}$ is shown in Fig. 3. The broad bands at 1950 and 2500 cm^{-1} are indicative of strong hydrogen bonding between the carboxylic acid group of PVTA and the pyridine nitrogen of $PHTC_6$ [24,35]. The formation of hydrogen bonds in other complexes are confirmed by FT-IR (Fig. S4 in Supplementary Content).

3.2. Thermal and LC properties of the complexes

The thermal and LC properties of the complexes were studied by DSC and PLM. Because TGA results show that the degradation temperatures of PVTA, PBCPS, and $PHTC_6$ are 276, 281, and 289 °C, respectively, the highest temperature in DSC measurements is only 240 °C. All the samples were first heated to 240 °C at a rate of 20 °C/min under a nitrogen atmosphere to erase the thermal history. Then DSC thermographs during the first cooling and second heating were obtained at a rate of 10 °C/min under a nitrogen atmosphere.

As shown in Fig. 4, two endothermic peaks and a broader

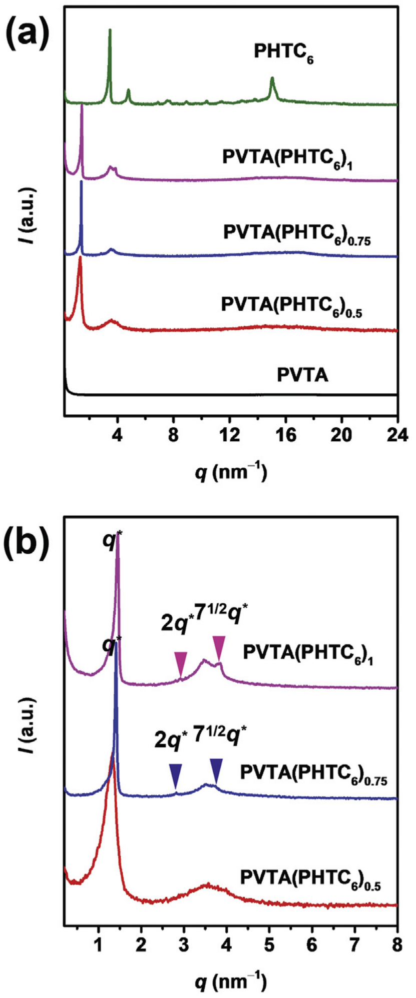

Fig. 6. SAXS profiles of $PHTC_6$, $PVTA(PHTC_6)_x$, and PVTA (a) and those of $PVTA_x$ in the low-angle region (b) with varying x.

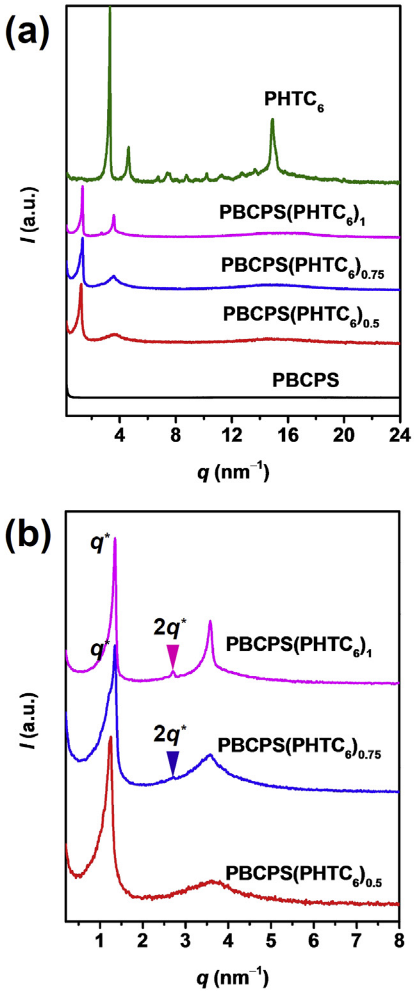

Fig. 7. SAXS profiles of $PHTC_6$, $PBCPS(PHTC_6)_x$, and PBCPS (a) and those of $PBCPS(PHTC_6)_x$ in the low-angle region (b) with varying x.

exothermic peak are observed during the second heating process for $PHTC_6$. Variable-temperature 1D WAXD results (Fig. S6 in Supplementary Content) indicate that with the increase of temperature the $PHTC_6$ molecule experiences a transformation from the crystalline state to the isotropic liquid directly when the temperature is above 100 °C. Therefore, the endothermic peak at 90 °C corresponds to the transition from the crystalline state to isotropic liquid. When the temperature increases from 30 °C to 80 °C, the high-angle diffraction peaks indicate crystalline structures. Thus, the exothermic peak at 50 °C corresponds to the transition between two crystalline phases. The similar transition has been observed in other triphenylene-based discotic molecules [36]. . However, no transition peaks are observed in the DSC curves of the complexes $PVTA(PHTC_6)_x$ and $PBCPS(PHTC_6)_x$, indicating that there is no macrophase separation and that no $PHTC_6$ crystalline phases are formed in the complexes.

PLM results show that all the complexes exhibit strong birefringence. The typical PLM micrographs of $PVTA(PHTC_6)_1$ and $PBCPS(PHTC_6)_1$ are shown in Fig. 5. However, no characteristic textures are observed.

3.3. Phase structure determination

In order to identify the phase structures of the complexes, SAXS and 2D WAXD experiments were performed. Samples for SAXS experiments were the bulk powders embedded in aluminum foils. In 2D WAXD experiments, oriented film specimens were obtained by shearing the bulk samples with a relatively large mechanical force at an appropriate temperature above the glass transition temperature (T_g) of the corresponding complex. All samples were thermally annealed overnight before measurements.

The phase behaviors of the complexes show a strong composition dependence. Figs. 6 and 7 show the SAXS results of $PVTA(PHTC_6)_x$ and $PBCPS(PHTC_6)_x$ at ambient temperature, respectively, with the profiles of pure PVTA, PBCPS, and $PHTC_6$ also included for comparison. For PVTA and PBCPS, there are no diffraction peaks in the high-angle region, which indicates that the pure PVTA and PBCPS are amorphous. The SAXS result of $PHTC_6$ also demonstrates that the pure $PHTC_6$ is crystalline at ambient temperature. As shown in Figs. 6a and 7a, there are no diffraction peaks in the profiles of the complexes in the high-angle region, indicating that $PHTC_6$ loses its crystalline structure when it is hydrogen-bonded with the MJPEs. On the other hand, there are only a few low-angle diffraction peaks that should be attributed to the complexes between the MJPEs and $PHTC_6$, revealing their LC nature. The amorphous halo in the high-angle region represents the characteristic dimensions of the amorphous packing of the alkyl chains along with the π–π stacking in Tp moieties. Therefore, the

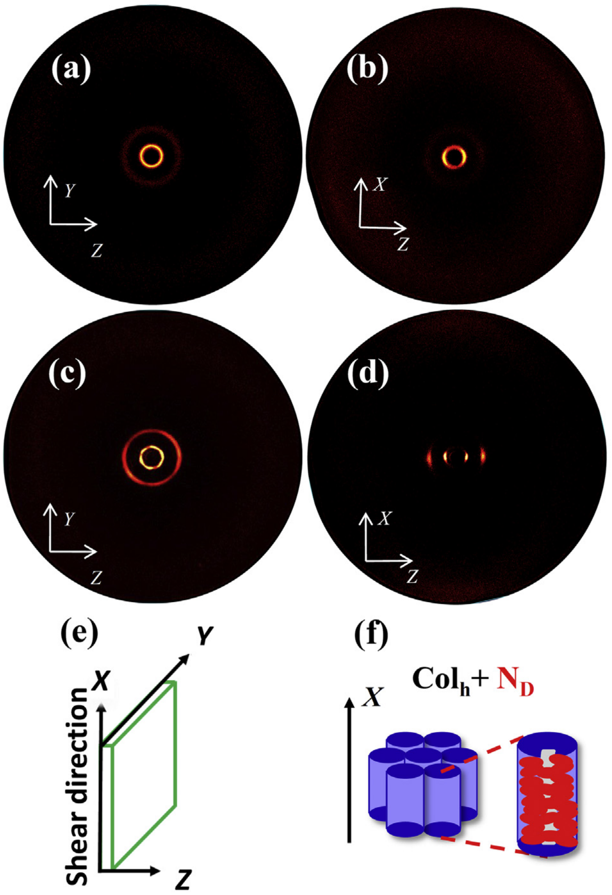

Fig. 8. 2D WAXD patterns of PVTA$(PHTC_6)_{0.5}$ (a, b) and PVTA$(PHTC_6)_1$ (c, d) with the X-ray incident beam parallel to the *X* (a, c) and *Y* (b, d) directions, the shearing geometry (e) and the sketch of the polymer chain structure (f).

intermolecular hydrogen bonding can prevent the crystallization of $PHTC_6$ and induce the ordering of the resultant complexes.

In Fig. 6b, the SAXS profile of PVTA$(PHTC_6)_x$, with $x = 0.5$, shows only one diffraction peak at $q = 1.33$ nm^{-1}, indicating the possible presence of a columnar phase. A broad scattering halo is also observed at about $q = 3.50$ nm^{-1} ($d = 1.79$ nm) in the low-angle region, which is the characteristic size of the Tp moiety [37,38]. When *x* is increased to 0.75, four diffraction peaks in the low-angle region are observed in the SAXS profile of PVTA$(PHTC_6)_x$. The halo at $q = 3.50$ nm^{-1} in PVTA$(PHTC_6)_{0.5}$ becomes a relatively broad peak, which means that the structure of the Tp moieties is more ordered with the increase in the content of $PHTC_6$. The peak with $q = q^*$ becomes sharper and stronger, and there is a *q* ratio of $1{:}2{:}\sqrt{7}$ for the three low-angle diffraction peaks except that at $q = 3.50$ nm^{-1} owing to the ordered packing of the Tp moieties, indicating the formation of a hexagonal columnar (Col_h) phase with the lattice parameter $a = 5.15$ nm that is not far away from the estimated dimension of 6.2 nm (assuming all *trans*-conformation of alkyl chains) of the side chain of PVTA$(PHTC_6)_x$ containing two Tp moieties, with the consideration of possible interdigitation of alkyl tails and even the Tp moieties. Therefore, the columnar phase is formed by the whole MJLCP containing Tp moieties as a supramolecular cylinder. When *x* is further increased to 1, a similar SAXS result to that of PVTA$(PHTC_6)_{0.75}$ is obtained, indicating that the LC phase of PVTA$(PHTC_6)_1$ is also Col_h. The lattice parameter *a* is 5.01 nm which is smaller than that of PVTA$(PHTC_6)_{0.75}$, suggesting that the complex with more Tp moieties is packed more closely.

Two-dimensional WAXD experiments were carried out to further verify the structures of the complexes. Parts a and b of Fig. 8 show 2D WAXD patterns of PVTA$(PHTC_6)_{0.5}$, with the X-ray incident beam parallel to the *X* and *Y* directions, respectively. In Fig. 8a, a sharp diffraction ring is observed near the beam stop. When the X-ray incident beam is parallel to the *Y* direction, the diffraction ring in Fig. 8a becomes two sharp diffraction arcs centered on the equator in Fig. 8b, suggesting a Col_n phase, which agrees well with the SAXS result. The position of diffraction arcs also indicates that the cylinders are parallel to the shear direction after mechanical shearing. Parts c and d of Fig. 8 show 2D WAXD patterns of PVTA$(PHTC_6)_1$. When the X-ray incident beam is parallel to the *X* direction, the first diffraction divided into six arcs with a 6-fold symmetry is observed near the beam stop in Fig. 8c, which confirms the existence of the Col_h phase. The second diffraction split into two arcs at $q = 3.49$ nm^{-1} (*d*-spacing = 1.80 nm) is originated from the structure (N_D phase) of the Tp moieties, and the close-to-ring pattern suggests the poor orientation of the Tp units in the *YZ* plane. When the X-ray incident beam is parallel to the *Y* direction, only two pairs of sharp diffraction arcs appear and are centered on the equator in Fig. 8d. Such a pattern indicates that the MJLCP columns are oriented parallel to the shear (*X*) direction, as expected. The diffraction associated with the characteristic dimension of the Tp moiety appears as a ring in Fig. 8c and on the equator in Fig. 8d, suggesting that the Tp discs are oriented with the disc normal parallel to the shear (*X*) direction. Considering the weak diffraction at $q = 3.50$ nm^{-1} in Fig. 6, the Tp moieties may be in an N_D or Col_n phase. However, it is quite difficult for the Tp discs, which are hydrogen-bonded to the main chain, to be packed into a Col_n phase in the matrix of a Col_h phase formed by the whole supramolecular polymer chain. Therefore, we assign the structure of the Tp moieties as an N_D phase. The 2D WAXD patterns of PVTA$(PHTC_6)_{0.75}$ are similar to those of PVTA$(PHTC_6)_1$ (Fig. S7 in Supplementary Content). The above results demonstrate that when $x \geq 0.75$ the complex PVTA$(PHTC_6)_x$ can form a hierarchical nanostructure in which the whole polymer chain serves as a cylinder to form the Col_h phase and the Tp moieties form an N_D phase within the columnar structure.

In Fig. 7b, the SAXS profiles of PBCPS$(PHTC_6)_x$ with $x = 0.5$ also show only one diffraction peak at $q = 1.25$ nm^{-1}, and the fact that it is a sharp and strong peak indicates the formation of a low-ordered smectic phase. In the low-angle region, a broad halo is also observed at $q \approx 3.57$ nm^{-1} ($d = 1.76$ nm), which is the characteristic size of the Tp moiety. The smectic phase of PBCPS$(PHTC_6)_{0.5}$ is different from the columnar structure of PVTA$(PHTC_6)_{0.5}$, which is consistent with our previous results that a more rigid side-chain core and a longer side chain increase the possibility of forming smectic phases for MJLCPs [39–41] With increasing content of $PHTC_6$, the halo at $q \approx 3.55$ nm^{-1} becomes a diffraction peak, implying that the Tp moieties in the side chains are packed in a more ordered fashion. In addition, this diffraction is stronger than that in Fig. 6, indicating that the degree of order of the structure formed by the Tp moieties in the PBCPS$(PHTC_6)_x$ ($x = 0.75$ and 1) complex is higher than in the PVTA$(PHTC_6)_x$ ($x = 0.75$ and 1) complex, even if the type of structure is the same. Furthermore, the *q* ratio of the other two low-angle diffraction peaks is 1:2, proving that the complexes PBCPS$(PHTC_6)_{0.75}$ and PBCPS$(PHTC_6)_1$ form smectic structures. The *d*-spacing values of the smectic structures of PBCPS$(PHTC_6)_{0.75}$ and PBCPS$(PHTC_6)_1$ are 4.65 nm, while The estimated dimension of the side chain of the MJLCP containing two Tp moieties is about 7.2 nm, which indicates significant interdigitation in the packing.

Fig. 9 shows the 2D WAXD patterns of PBCPS$(PHTC_6)_x$. Parts a and b show 2D WAXD patterns of PBCPS$(PHTC_6)_{0.5}$, with the X-ray incident beam parallel to the *X* and *Y* directions, respectively. There

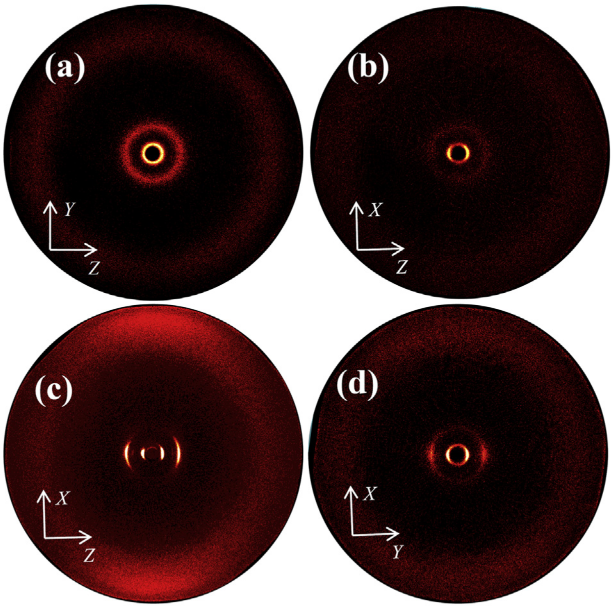

Fig. 9. 2D WAXD patterns of PBCPS$(PHTC_6)_{0.5}$ with the X-ray incident beam parallel to the X (a) and Y (b) directions and those of PBCPS$(PHTC_6)_1$ with the X-ray incident beam parallel to the Y (c) and Z (d) directions.

is a sharp diffraction ring in Fig. 9a, and there are a pair of sharp diffraction arcs on the equator in Fig. 9b, consistent with a low-ordered smectic phase. However, there is only an amorphous diffuse ring in the high-angle region, which is hard to determine whether the smectic phase is smetic A (SmA) or smetic C (SmC). The 2D WAXD patterns of PBCPS$(PHTC_6)_1$ are shown in parts c and d of Fig. 9, with the X-ray incident beam parallel to the Y and Z directions, respectively. In both 2D WAXD patterns, three pairs of sharp diffraction arcs located on the equator are observed. The q ratio of the two pairs of diffraction arcs other than that at $q = 3.57\ \mathrm{nm}^{-1}$ (d-spacing $= 1.76$ nm) is 1:2, demonstrating a smectic structure. The pair of diffuse arcs in the high-angle region is centered on the meridian, indicating an SmA phase. Similar to the case of PVTA$(PHTC_6)_x$ ($x = 0.75$ and 1) complex, the Tp moieties are also likely to form the N_D phase in the SmA matrix. The appearance of the pair of diffraction arcs with $q = 3.57\ \mathrm{nm}^{-1}$ on the equator suggests that the Tp discs are also oriented with the disc normal parallel to the shear direction. Therefore, the normal of the Tp discs are perpendicular to the layer normal of the SmA structure. The 2D WAXD patterns of PBCPS$(PHTC_6)_{0.75}$ (Fig. S7 in Supplementary Content) are similar to those of PBCPS$(PHTC_6)_1$. Therefore, the PBCPS$(PHTC_6)_x$ ($x = 0.75$ and 1) complex also forms a hierarchical nanostructure in which the whole polymer chain serves as a supramolecular tablet to form the SmA phase and the Tp moieties develop an N_D phase within the smectic structure. In addition, from the SmA phases of PBCPS$(PHTC_6)_{0.75}$ and PBCPS$(PHTC_6)_1$, we propose that PBCPS$(PHTC_6)_{0.5}$ also forms a SmA phase.

Because the hierarchical nanostructures of the complexes with $x \geq 0.75$ are induced by the introduction of the Tp moieties, we investigated the influence of the isotropization of the Tp moieties upon heating on the phase behaviors of the complexes. Variable-temperature SAXS results of PVTA$(PHTC_6)_1$ and PBCPS$(PHTC_6)_1$ are shown in parts a and b of Fig. 10, respectively. When the complexes are heated to 150 °C, the diffraction peak at $q \approx 3.50\ \mathrm{nm}^{-1}$ attributed to the ordered structure of the Tp moieties becomes an amorphous halo, indicating that the Tp moieties are in the isotropic state. In Fig. 10a, the peak with $q = q^*$ becomes broader and weaker than that at low temperatures, suggesting that PVTA$(PHTC_6)_1$ transforms from the Col_h phase to the Col_n phase when the Tp moieties isotropilize. The hydrogen bonds are still present during the heating process from variable-temperature FT-IR results (Fig. S8 in Supplementary Content). In Fig. 10b, the peak with $q = q^*$ remains sharp compared to those at low temperatures, which implies that the smectic phase of PBCPS$(PHTC_6)_1$ remains, while the broadening of the peak demonstrates that the degree of order is decreased when the Tp moieties go to isotropic. Such a difference in the phase behaviors of PVTA$(PHTC_6)_1$ and PBCPS$(PHTC_6)_1$ can again be attributed to the different rigidities and lengths of the main chains in these two complexes. In both types of complexes, the degree of order of the low-temperature larger-scale structure is higher than that of the phase at high temperatures when Tp goes into isotropic, suggesting that the N_D phase at low temperatures improves the structure of the whole supramolecular polymer chain or that alternatively the more ordered structure of the whole polymer renders the ordered packing of the Tp moieties. In other words, the two types of mesogens are promotive to each other, as in the covalent analogs [21].

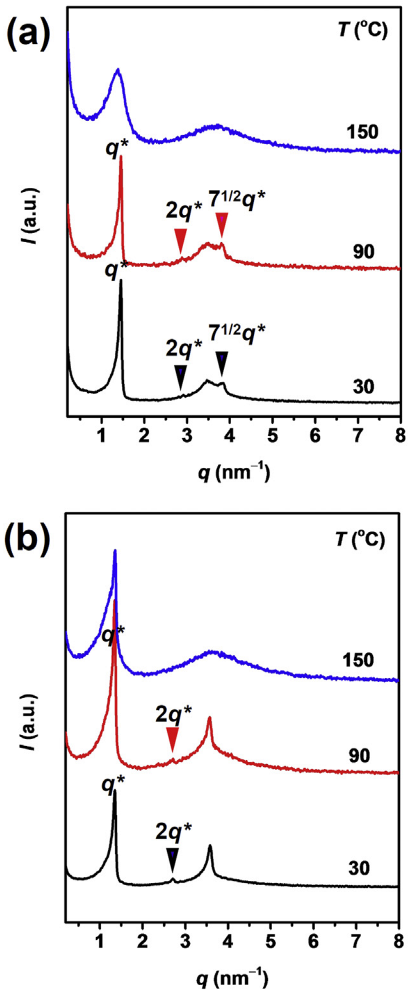

Fig. 10. SAXS profiles of PVTA$(PHTC_6)_1$ (a) and PBCPS$(PHTC_6)_1$ (b) at different temperatures during heating.

Fig. 11 depicts the schematic representation of the phase structures of the hydrogen-bonded complexes at low temperatures with varying contents of $PHTC_6$. As demonstrated by the above-mentioned results, the complexes exhibit complicated phase

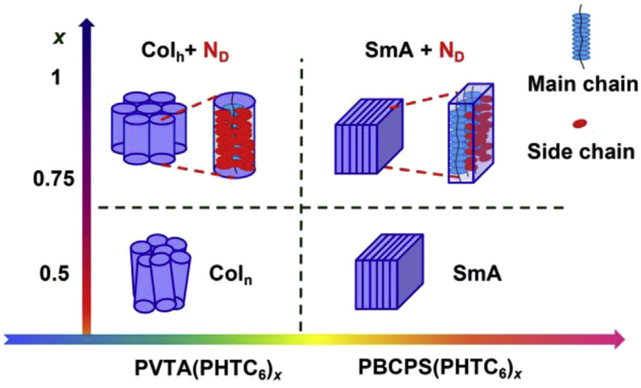

Fig. 11. Schematic drawing of the phase structures of the hydrogen-bonded complexes at low temperatures.

behaviors involving both the competition and the synergistic effect between the two different LC mesogens. With increasing x up to 1, the phase structure of PVTA($PHTC_6$)$_x$ transforms from a simple Col_n phase to a hierarchical nanostructure containing a Col_h phase formed by the whole polymer chains and an N_D phase attributed to the Tp moieties, while the phase structure of PBCPS($PHTC_6$)$_x$ changes from a simple SmA phase to a hierarchical nanostructure containing an SmA phase originated from the whole polymer chains and an N_D phase owing to the Tp moieties. Therefore, we propose that the complexes behave more like individual MJLCPs and that the Tp moieties can be simply regarded as the component of the side chains of the MJLCPs when the content of $PHTC_6$ is relatively low and the interaction between the Tp moieties is weak. With increasing content of $PHTC_6$, the interaction between the Tp moieties becomes stronger, and both types of LC mesogens can act more independently to display their individual self-organizing structures. As mentioned previously, the difference in the rigidity of the MJLCP side chains leads to the different LC phase structures of PVTA($PHTC_6$)$_x$ and PBCPS($PHTC_6$)$_x$. The rigid core of the side chain in PBCPS($PHTC_6$)$_x$ has three benzene rings, resulting in stronger steric hindrance in PBCPS($PHTC_6$)$_x$ compared with that in PVTA($PHTC_6$)$_x$ containing only one benzene ring in the side-chain core.

4. Conclusions

In conclusion, we obtained two series of MJLCP-based supramolecular MCSCLCPs via hydrogen bonding. Two MJPEs with different side groups were synthesized as hydrogen-bonding donors, and a pyridine derivative containing a Tp unit was synthesized as the hydrogen-bonding acceptor. The intermolecular hydrogen bonds between the MJPEs and $PHTC_6$ are confirmed by FT-IR results. In addition to the dependence on temperature, the phase behaviors of the hydrogen-bonded complexes are also influenced by the molar ratio x and the MJPE main chain. As supramolecular MJLCPs, the two complexes form a Col_n or an SmA phase depending on the total length or the rigidity of the side chain containing two Tp moieties. When $x = 0.5$, the complexes only exhibit a simple columnar or smectic LC phase. When $x \geq 0.75$, the Tp moieties form an N_D phase, leading to a hierarchical nanostructure. In addition to the competition between the packing of the two different types of mesogens, namely, the MJLCP and the discotic Tp, variable-temperature SAXS results prove that these two types of mesogens are also promotive to each other. Our work proves that we can prepare MJLCP-based MCSCLCPs via hydrogen bonding, resulting in simplified design and synthesis of new MCSCLCPs, which is of great importance for fundamental research in the fields of LCPs and supramolecular chemistry. This supramolecular method provides a facile approach to regulating ordered hierarchical nanostructures and exploring new functional materials.

Acknowledgment

This work is supported by the National Natural Science Foundation of China (Grants: 21174006 and 20990232).

Appendix A. Supplementary data

Supplementary data related to this article can be found at http://dx.doi.org/10.1016/j.polymer.2016.01.018.

References

[1] T. Kato, N. Mizoshita, K. Kishimoto, Angew. Chem. Int. Ed. Engl. 45 (1) (2006) 38–68.
[2] D.L. Thomsen, P. Keller, J. Naciri, R. Pink, H. Jeon, D. Shenoy, B.R. Ratna, Macromolecules 34 (17) (2001) 5868–5875.
[3] B.R. Kaafarani, Chem. Mater. 23 (3) (2010) 378–396.
[4] M. O'Neill, S.M. Kelly, Adv. Mater. 23 (5) (2011) 566–584.
[5] A. Buguin, M.-H. Li, P. Silberzan, B. Ladoux, P.J. Keller, Am. Chem. Soc. 128 (4) (2006) 1088–1089.
[6] W. Pisula, M. Zorn, J.Y. Chang, K. Müllen, R. Zentel, Macromol. Rapid Commun. 30 (14) (2009) 1179–1202.
[7] B.R. Maughon, M. Weck, B. Mohr, R.H. Grubbs, Macromolecules 30 (2) (1997) 257–265.
[8] R.P. Nieuwhof, A. Koudijs, A.T.M. Marcelis, E.J.R. Sudhölter, Macromolecules 32 (20) (1999) 6499–6506.
[9] T. Ranganathan, C. Ramesh, A.J. Kumar, Polym. Sci. A Polym. Chem. 42 (11) (2004) 2734–2746.
[10] S. Jin, K.-U. Jeong, Y. Tu, M.J. Graham, J. Wang, F.W. Harris, S.Z.D. Cheng, Macromolecules 40 (15) (2007) 5450–5459.
[11] R. Zentel, M. Brehmer, Acta Polym. 47 (4) (1996) 141–149.
[12] B. Reck, H. Ringsdorf, Macromolecules 6 (4) (1985) 291–299.
[13] N.F. Cooray, H. Fujimoto, M-a Kakimoto, Y. Imai, Macromolecules 30 (11) (1997) 3169–3174.
[14] S.-H. Joo, Y.-K. Yun, J.-I. Jin, D.-C. Kim, W.-C. Zin, Macromolecules 33 (18) (2000) 6704–6712.
[15] W. Huang, C.D. Han, Macromolecules 39 (14) (2006) 4735–4745.
[16] K.E. Schaefer, P. Keller, T.J. Deming, Macromolecules 39 (1) (2005) 19–22.
[17] Q.F. Zhou, H.M. Li, X.D. Feng, Macromolecules 20 (1) (1987) 233–234.
[18] Q. Zhou, X. Zhu, Z. Wen, Macromolecules 22 (1) (1989) 491–493.
[19] H.L. Xie, T.H. Hu, X.F. Zhang, H.L. Zhang, E.Q. Chen, Q.F. Zhou, J. Polym. Sci. A Polym. Chem. 46 (22) (2008) 7310–7320.
[20] H.-L. Xie, C.-K. Jie, Z.-Q. Yu, X.-B. Liu, H.-L. Zhang, Z. Shen, E.-Q. Chen, Q.-F. Zhou, J. Am. Chem. Soc. 132 (23) (2010) 8071–8080.
[21] Y.-F. Zhu, X.-L. Guan, Z. Shen, X.-H. Fan, Q.-F. Zhou, Macromolecules 45 (8) (2012) 3346–3355.
[22] Y.F. Zhu, H.J. Tian, H.W. Wu, D.Z. Hao, Y. Zhou, Z.H. Shen, D.C. Zou, P.C. Sun, X.H. Fan, Q.F. Zhou, J. Polym. Sci. A Polym. Chem. 52 (3) (2014) 295–304.
[23] T. Kato, J.M.J. Frechet, Macromolecules 22 (9) (1989) 3818–3819.
[24] T. Kato, H. Kihara, T. Uryu, A. Fujishima, J.M.J. Frechet, Macromolecules 25 (25) (1992) 6836–6841.
[25] U. Kumar, T. Kato, J.M.J. Frechet, J. Am. Chem. Soc. 114 (17) (1992) 6630–6639.
[26] T. Kato, O. Ihata, S. Ujiie, M. Tokita, J. Watanabe, Macromolecules 31 (11) (1998) 3551–3555.
[27] M. Gopinadhan, E.S. Beach, P.T. Anastas, C.O. Osuji, Macromolecules 43 (16) (2010) 6646–6654.
[28] S.J. Wang, Y.S. Xu, S. Yang, E.Q. Chen, Macromolecules 45 (21) (2012) 8760–8769.
[29] Y. Xu, W. Qu, Q. Yang, J. Zheng, Z. Shen, X. Fan, Q. Zhou, Macromolecules 45 (6) (2012) 2682–2689.
[30] L.-C. Gao, C.-L. Zhang, X. Liu, X.-H. Fan, Y.-X. Wu, X.-F. Chen, Z. Shen, Q.-F. Zhou, Soft Matter 4 (6) (2008) 1230–1236.
[31] Y. Xu, Q. Yang, Z. Shen, X. Chen, X. Fan, Q. Zhou, Macromolecules 42 (7) (2009) 2542–2550.
[32] D. Zhang, Y.-X. Liu, X.-H. Wan, Q.-F. Zhou, Macromolecules 32 (16) (1999) 5183–5185.
[33] W. Qu, X. Zhu, J. Chen, L. Niu, D. Liang, X. Fan, Z. Shen, Q. Zhou, Macromolecules 47 (8) (2014) 2727–2735.
[34] C.M. Xing, J.W.Y. Lam, K.Q. Zhao, B.Z. Tang, J. Polym. Sci. A Polym. Chem. 46 (9) (2008) 2960–2974.
[35] J.Y. Lee, P.C. Painter, M.M. Coleman, Macromolecules 21 (4) (1988) 954–960.
[36] S. Kumar, Liq. Cryst. 31 (8) (2004) 1037–1059.
[37] X.L. Piao, J.-S. Kim, Y.-K. Yun, J.-I. Jin, S.-K. Hong, Macromolecules 30 (8) (1997)

2294–2299.
[38] Z.Q. Yu, J.W.Y. Lam, K.Q. Zhao, C.Z. Zhu, S. Yang, J.S. Lin, B.S. Li, J.H. Liu, E.Q. Chen, B.Z. Tang, Polym. Chem. 4 (4) (2013) 996–1005.
[39] X.-F. Chen, Z. Shen, X.-H. Wan, X.-H. Fan, E.-Q. Chen, Y. Ma, Q.-F. Zhou, Chem. Soc. Rev. 39 (8) (2010) 3072–3101.
[40] S. Chen, L.C. Gao, X.D. Zhao, X.F. Chen, X.H. Fan, P.Y. Xie, Q.F. Zhou, Macromolecules 40 (16) (2007) 5718–5725.
[41] C.P. Chai, X.Q. Zhu, P. Wang, M.Q. Ren, X.F. Chen, Y.D. Xu, X.H. Fan, C. Ye, E.Q. Chen, Q.F. Zhou, Macromolecules 40 (26) (2007) 9361–9370.